Presented at the 22nd European Photovoltaic Solar Energy Conference and Exhibition, 3.-7. September 2007, Milano

SILICON SOLAR CELLS WITH SCREEN-PRINTED FRONT SIDE METALLIZATION EXCEEDING 19% EFFICIENCY

O. Schultz[1], A. Mette[1,2], R. Preu[1], S.W. Glunz[1]

[1]Fraunhofer ISE, Heidenhofstrasse 2, 79110 Freiburg, Germany,
Phone ++761-4588-5355; Fax ++761-4588-9250, email: Oliver.Schultz@ise.fraunhofer.de
[2]Now with Q-Cells AG, Germany

ABSTRACT: Thermal oxides are commonly used for the surface passivation of high-efficiency crystalline silicon solar cells and have led to the highest conversion efficiencies of mono- and multicrystalline silicon reported so far. In contrast to the laboratory fabrication of solar cell structures with lithographically defined and evaporated front contacts, in this study we combine several technologies ready for industrial implementation. On the front side, surface passivation of the lowly doped emitters up to 90 Ω/sq is achieved with sputtered SiN_x:H, the contact grid is created with screen-printing of a hotmelt silver paste, the electrical properties of the grid are improved by light-induced silver plating. Since contact formation on the front requires a short high-temperature firing process, the rear surface passivation layer needs to be thermally stable. A wet thermal oxidation is applied on the rear and the surface recombination velocity of the fired oxide is experimentally determined to be below $S \leq 38$ cm/s at the end of the process sequence. This includes evaporation of aluminium on the rear, the formation of laser-fired contacts and a short annealing process under air ambience. Monocrystalline solar cells were produced and 19.3% efficiency were obtained as best value on 4 cm^2 cell area.

Keywords: High-Efficiency, Silicon Solar Cells, Screen-Printing

1 INTRODUCTION

In order to improve the cost-effectiveness of solar cells from mono- and multicrystalline silicon, the efficiency has to be increased and wafer thickness has to be reduced. One very important component of the cell influencing the performance especially for thin wafers is the rear surface. The increasing demands for optical quality require a higher internal reflection and also the electrical quality can be improved applying a more sophisticated surface passivation than a full-area aluminium back-surface field (Al-BSF). Therefore, all designs for high-efficiency silicon solar cells today feature a dielectric passivation layer on the rear. Provided that the refractive index of this layer is low enough, this results in a very good optical mirror with high internal reflection. This leads to a good light-trapping that can be further improved by evaporation of a thin layer of aluminium. To extract the carriers from the cell, a point-contact pattern has proven sufficient for good carrier collection [1]. Both cell structures are sketched in Figure 1. A very good surface passivation is required in order to realise an efficiency gain of the passivated rear in comparison to a full-area contacted screen-printed Al-BSF.

A common technology meeting the requirements of passivation quality and optical properties is a thick thermal oxidation (≥100 nm) at high temperatures. This has led to the highest conversion efficiencies on monocrystalline silicon so far [2]. A technological modification of the standard oxides grown at 1050°C in dry ambience is the use of pyrogenic steam [3]. This increases the growth rate and/or reduces the oxidation temperature. The latter is especially beneficial for high-temperature sensitive material and enabled the first cells in excess of 20% efficiency on multicrystalline silicon using a process at 800°C [4]. This wet oxidation is about one order of magnitude faster than the dry oxidation process and therefore a viable technology for industrial silicon solar cell processing.

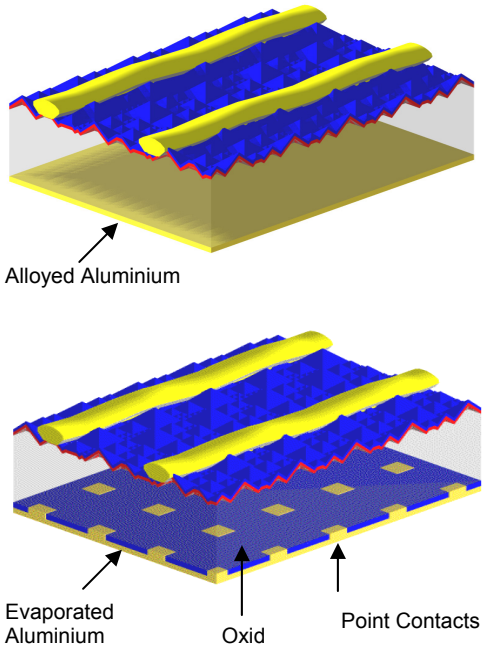

Fig. 1: Solar cell structures with screen-printed front metallization and full area Al-BSF (top) and passivated rear with point contacts (bottom)

Following the development of high-efficiency cells using photolithography technology, in the present study cells are manufactured employing an industrial front structure with screen-printed contacts. The front surface consists of a phosphorus doped emitter passivated by a single layer antireflection coating of silicon nitride (SiN_x:H). The contact grid is screen-printed hotmelt silver paste [5], which needs to be fired through the SiN_x-

layer. This short high-temperature process of 800°C - 900°C can potentially degrade passivation layers. Therefore, a good process design needs to take into account the passivation quality at the end of the process sequence, i.e. the rear passivation layer has to be temperature stable.

The question to be answered is: Can a wet thermal oxide yield low rear surface recombination velocities and withstand the firing process?

2 EXPERIMENTS

2.1 Thermal stability of thermal oxide for rear surface passivation

Bright-etched boron-doped FZ silicon wafers of 1 Ω cm base resistivity and of 330 µm thickness were cleaned and oxidised in steam ambience. The wafers were fired in an inline belt furnace at the same settings like they were used in solar cell fabrication (see next section). Then aluminium of 2 µm thickness was evaporated on both sides and the wafers were annealed at 350°C for 15 min before the metallic layers were etched off in hydrochloric acid. The effective carrier lifetime of the samples was measured with the QssPC technique [6]. The average lifetime was 335 µs. Evaluation according to equation

$$\frac{1}{\tau_{eff}} \cong \frac{1}{\tau_{bulk}} + \frac{2S}{W}$$

with the assumption of τ_{bulk} = 1500 µs results in an upper limit of S ≤ 38 cm/s. This can be converted to 54 cm/s for 0.5 Ω cm material [7]. Applying laser-fired contacts with a contact pitch of 750 µm, this results in effective surface recombination velocities of S_{eff} = 112 cm/s and 143 cm/s, respectively [8].

Although the recombination velocities are significantly higher than the values derived for the wet oxide without the firing process [9], this is low enough to provide excellent surface passivation and allows for highly efficient solar cells. Therefore, the oxide was implemented in the process sequence as described in the following section.

2.2 Process sequence

In order to test the cell structure, high-quality boron-doped FZ silicon of 0.5 Ω cm base resistivity and 250 µm thickness was used as a substrate for seven cells of 4 cm^2 aperture area on each wafer. Both, cells with a standard industrial Al-BSF and cells with an oxide passivation were processed in order to experimentally determine the benefit of the point-contacted oxide-passivated rear compared to the full-area Al-BSF. Recently developed technologies for crystalline silicon solar cell production like wet oxidation [4], sputtering of silicon nitride [10], screen-printing of hotmelt silver paste [5], laser-fired contacts [11] and light-induced silver plating [12] were implemented in an industrial process sequence shown in Figure 2 resulting in the cell structures shown in Figure 1. The thermal oxide was applied at the very beginning of the process sequence and grown thick enough to withstand the random pyramid etching, to mask the local $POCl_3$-diffusion and to resist the short etching of the phosphorus glass.

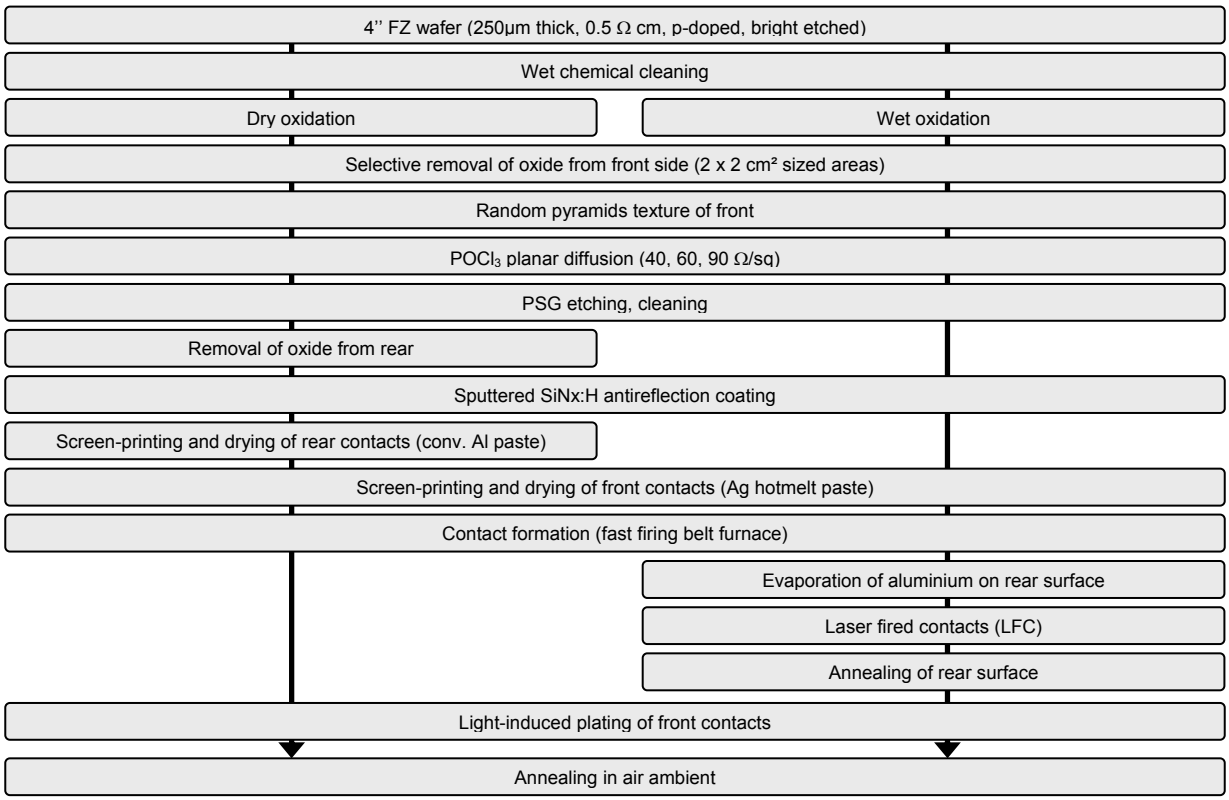

Fig. 2: Process flow diagram of manufactured solar cells featuring screen-printed front contacts thickened by light-induced plating. The left flow shows the Al-BSF process, on the right-hand side the rear side is passivated by wet thermal oxide.

This has the advantage that the rear surface is covered during the whole process sequence and no emitter etch-back nor sophisticated cleaning processes have to be applied except at the very beginning.

2.3 Results

The results of the *IV*-measurements of the best cells under standard testing conditions are shown in Table 1.

Table 1: *IV*-parameters of the best solar cells with Al-BSF or oxide passivated rear.
*Calibrated measurement at Fraunhofer ISE Calibration Laboratory

R_{sh} [Ω/sq]	rear side	V_{oc} [mV]	j_{sc} [mA/cm^2]	FF [%]	η [%]
40	Al-BSF	632	35.2	81.2	18.1
	Oxide	639	36.7	80.0	18.8
60	Al-BSF	632	35.6	81.2	18.3
	Oxide	647	37.1	79.6	19.1
90	Al-BSF	640	36.5	79.8	18.7
	Oxide	655	38.2	76.9	19.3*

For all emitter diffusions the V_{oc} and j_{sc} values are significantly increased for the oxide passivated cells. For further analysis the quantum efficiency and reflectance measurements are shown in Figure 3.

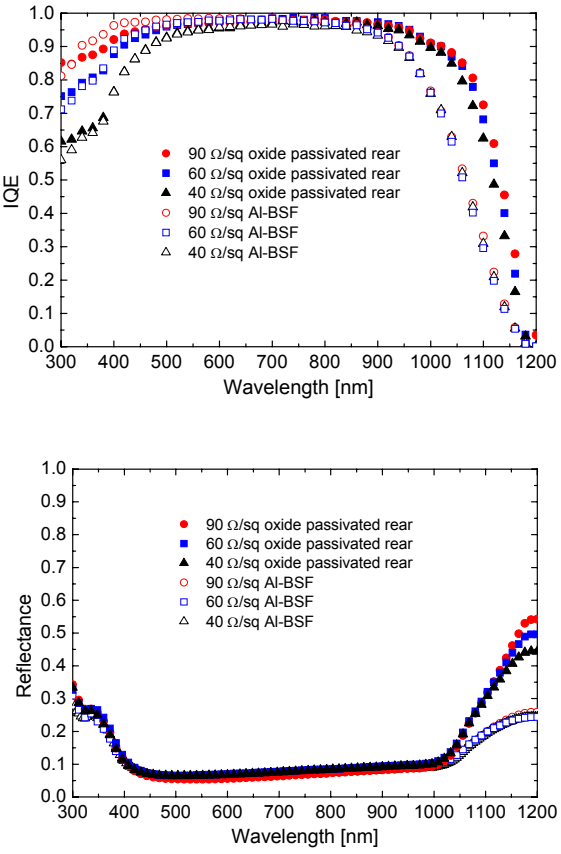

Fig. 3: Measurement of internal quantum efficiency IQE and reflectance for the Al-BSF and for the oxide passivated rear.

In the short wavelength region, and therefore linked to the properties of the front surface of the cells, the difference in the quantum efficiency is due to the different emitter doping profiles and thus the two types of cell structure show nearly equal performance. In the long wavelength region, representing the rear surface properties, the Al-BSF and the oxide passivated cells exhibit distinct differences. The superior rear surface passivation and the high internal reflectance lead to a significant gain in the short-circuit current density and open-circuit voltage compared to the Al-BSF cells. Additionally, differences in the reflectance between 1150 nm and 1200 nm can be observed for the three different emitters. This can be attributed to free-carrier absorption of the long-wavelength photons in the highly doped emitter layers.leading to slightly higher quantum efficiencies for the 60 Ω/sq and 90 Ω/sq emitter also in the long-wavelength region.

The fill factor *FF* of the point-contacted cell is slightly lower than the fill factor of the full-area contacted Al-BSF. This can be explained by increased series resistance on the rear due to the point-contact structure and increased spreading-resistance [13, 14]. The differences in *FF* are small for the 40 Ω/sq and the 60 Ω/sq emitter, for the 90 Ω/sq the difference cannot be explained by the cell design but must be due to a technological problem. However, the high gain in j_{sc} and V_{oc} still allow a gain of 0.6% absolute. An electrical conversion efficiency of 19.3% was measured in a calibrated measurement at Fraunhofer ISE CalLab. This efficiency is, to the knowledge of the authors, the highest value reported for a screen-printed front metallization pattern to date [15].

2.4 Simulation

In order to assess the potential of the cells structure and the process, 1-dimensional modelling using PC1D [16] was performed for the cells with 60 Ω/sq emitter. The doping profile was measured by SIMS and used for the Al-BSF and the oxide passivated rear. First, the reflectance was simulated by adjusting the internal reflectance values in PC1D in a way that a good fit was obtained. This resulted in $R_{back} = 66\%$ (diffuse) on the rear for the cell with Al-BSF and $R_{back} = 92\%$ (specular) for the oxide passivated one.

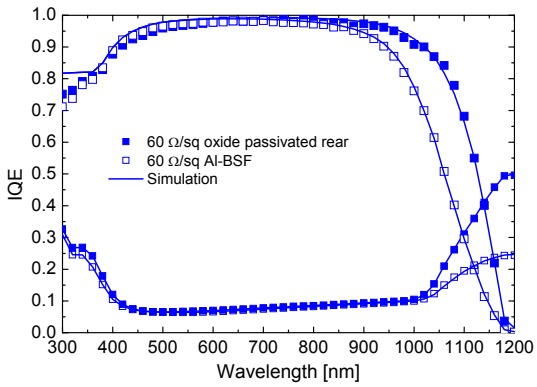

Fig. 4: Simulated internal quantum efficiency and reflectance (lines) fitted to the measurements (dots).

Then the rear surface recombination velocity S_{eff} of the Al-BSF cell was adjusted. In order to obtain a good fit of the measured quantum efficiency a value of S_{eff} =900 cm/s was chosen. For the oxide passivated cell the value of S_{eff} = 143 cm/s calculated in section 2.1 was used and allowed a good description of the measured data. In both cases a bulk lifetime of τ_{bulk} = 500 µs was assumed. The simulation results are displayed in Fig. 4, the main fit parameters for the 60 Ω/sq. cells are summarized in Table 2.

Table 2: Internal reflectivities (R_{back}) and effective rear surface recombination velocities at the back (S_{eff}) as extracted from solar cell modelling ((d) = diffuse and (s) specular reflection). In addition the j_{sc} and V_{oc} simulation results are presented. The simulation was performed on cells with 60 Ω/sq emitter.

Rear side	R_{back} [%]	S_{eff} [cm/s]	V_{oc} [mV]	j_{sc} [mA/cm^2]
Al-BSF	66 (d)	900	637	35.5
oxide	92 (s)	143	645	37.1

The relative gain by using the oxide passivation instead of a full-area Al-BSF is shown in Figure 5. According to the simulation, the improved rear surface passivation and higher internal reflectance increase V_{oc} and j_{sc} by 1.3% and 4.5%, respectively. The difference in *FF* was experimentally determined to be 2% relative. Overall, a relative gain in efficiency of 3.8% for a standard 60 Ω/sq emitter is calculated, this gain will increase for even lower doped emitters.

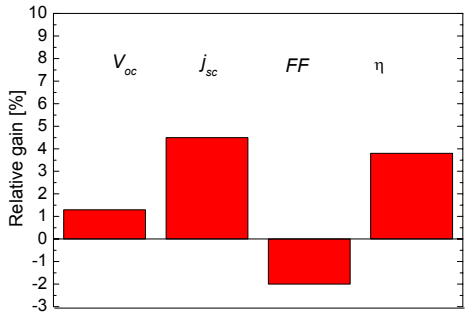

Fig.5: Simulation results illustrating the relative gain of solar cell parameters by using the oxide passivation instead of a full area Al-BSF. Modelling refers to a 240 µm thick solar cell with a base doping of 0.5 Ω cm and an emitter sheet resistance of 60 Ω/sq.

3 SUMMARY

A wet thermal oxide was implemented in the beginning of an industrial-like process sequence. It served as a masking layer against random pyramid texturing and $POCl_3$ emitter diffusion. The front contacts were formed with screen-printed and fired silver paste. After aluminium annealing of the rear, excellent surface recombination velocities of $S \leq$ 38 cm/s were measured. In combination with laser-fired contacts effective rear surface recombination velocities of S_{eff} =143 cm/s on 0.5Ω cm base resistivity were calculated for a contact pitch of 750 µm. Solar cells of 4 cm^2 aperture area were fabricated and efficiencies in excess of 19% were reached for emitter sheet resistances of 60 Ω/sq and 90 Ω/sq.

ACKNOWLEDGEMENT

The authors would like to thank all members of the Fraunhofer ISE Solar Cell Department for their contributions to this work.

REFERENCES

[1] A.W. Blakers and M.A. Green, Applied Physics Letters **48** (1986) 215
[2] J. Zhao, A. Wang and M.A. Green, Progress in Photovoltaics: Research and Applications **7** (1999) 471
[3] M. Stocks and A. Cuevas, Proceedings of the 2nd World Conference on Photovoltaic Energy Conversion, Vienna, Austria (1998) 1623
[4] O. Schultz, S.W. Glunz and G.P. Willeke, Progress in Photovoltaics: Research and Applications **12** (2004) 553
[5] A. Mette, D. Erath, R. Ruiz, G. Emanuel, E. Kasper and R. Preu, Proceedings of the 20th European Photovoltaic Solar Energy Conference, Barcelona, Spain (2005) 873
[6] R.A. Sinton and A. Cuevas, Applied Physics Letters **69** (1996) 2510
[7] O. Schultz Dissertation, Fakultät für Physik, Universität Konstanz, Konstanz 2005
[8] D. Kray and S.W. Glunz, Progress in Photovoltaics: Research and Applications **14** (2006); 195
[9] O. Schultz, S.W. Glunz, D. Kray, M. Dhamrin, I. Yamaga, T. Saitoh and G.P. Willeke, Proceedings of the 20th European Photovoltaic Solar Energy Conference, Barcelona, Spain (2005) 741
[10] W. Wolke, J. Catoir, R. Preu, G. Emanuel, J. Liu, M. Ruske, Proceedings of the 20th European Photovoltaic Solar Energy Conference, Barcelona, Spain (2005) 733
[11] E. Schneiderlöchner, R. Preu, R. Lüdemann and S.W. Glunz, Progress in Photovoltaics: Research and Applications **10** (2002) 29
[12] A. Mette, C. Schetter, D. Wissen, S. Lust, S.W. Glunz and G. Willeke, Proceedings of the 4th World Conference on Photovoltaic Energy Conversion, Waikoloa, Hawaii, USA (2006) 1056
[13] K.R. Catchpole and A.W. Blakers, Proceedings of the 16th European Photovoltaic Solar Energy Conference, Glasgow, UK (2000) 1719
[14] B. Fischer, Dissertation, Fakultät für Physik, Universität Konstanz, Konstanz 2003
[15] M.M. Hilali, K. Nakayashiki, A. Ebong and A. Rohatgi, Progress in Photovoltaics: Research and Applications **14** (2006); 135
[16] D.A. Clugston and P.A. Basore, Proceedings of the 26th IEEE Photovoltaic Specialists Conference, Anaheim, California, USA (1997) 207